26.7 A 10mm³ Syringe-Implantable Near-Field Radio System on Glass Substrate

Yao Shi, Myungjoon Choi, Ziyun Li, Gyouho Kim, Zhiyoong Foo, Hun-Seok Kim, David Wentzloff, David Blaauw

University of Michigan, Ann Arbor, MI

We present a millimeter-scale near-field radio system for ultra-low-power (ULP) healthcare sensor nodes. It is specifically designed for 'syringe implantation' which minimizes invasiveness of implantation. Designing a millimeter-scale wireless node for implanted healthcare is challenging because: 1) the antenna is constrained to the diameter of the syringe needle, which significantly constrains the link distance through RF. 2) The energy/power are strictly limited by the millimeter-scale form-factor where thin-film batteries can source only <10μAh and sustain <50μA peak current. Recent works [1-4] have demonstrated near-field transceivers for millimeter-scale implants. Passive backscatter radios consume low power but they are only operable at very short distances (e.g., 3.5cm) due to excessive path loss and self-jamming at the reader [1-2]. Although active radios can provide >10cm distance, their high power consumption (45mW [3]) and/or large antenna size (2.3cmx2.4cm [4]) make them impractical for implanted healthcare applications.

We propose three major techniques to realize a ULP millimeter-scale implanted sensor node communication: 1) a co-optimized, asymmetric magnetic antenna pair on the implanted sensor node and the base-station device, 2) a pulse-inject H-bridge LC-oscillator with improved efficiency that replaces a conventional constant-bias cross-coupled LC-oscillator [3-5], and 3) a new sensor-initiating synchronization protocol where accurate timing offset estimation is performed on the base-station eliminating the necessity of an area-demanding off-chip crystal and synchronization baseband processing on the sensor node, significantly improving its energy efficiency. Combining these techniques, the proposed system achieves a link distance up to 50cm (sensor TX) and 20cm (sensor RX), including 3cm of tissue. We integrated the transceiver, baseband controller, timer, wakeup controller and MBUS communication controller [6] on a single chip, together with a 1x8mm^2 magnetic antenna fabricated with 1.5μm-thickness gold on 100μm-thickness glass substrate (Fig. 26.7.1). The overall system volume (1x1x10 mm^3) fits in a 14-gauge syringe needle. When powered by a 1x2.21mm^2 thin-film battery (2μAh, 4.1V), the designed system has a 2-week expected lifetime without battery recharging, when the system wakes up, transmits and receive 16b data every 10 minutes.

The antenna dimension of the implantable sensor node is strictly limited, while the antenna on the base-station is less constrained. The resonant coupling strength between these two antennas (Fig. 26.7.2), is determined by their mutual inductance, Q factor, and resonant frequency. Given 1mm coil width, extensive HFSS simulations show that the coupling strength increases with longer antenna length. However, beyond 1x8mm^2 increase in mutual inductance is offset by lower self-resonant frequency (SRF) and Q-factor and coupling strength saturates. 15 turns (0.6 fill-factor) was found to be optimal in simulations with an SRF of 118MHz. It corresponds well with 114.7MHz RF-probe-testing measurement (Fig. 26.7.2, left) and 112MHz measured from the integrated system. The base-station antenna dimension is 11x11cm^2, which is driven by its carrier frequency and Q factor. We propose asymmetric transmit-signal power levels and carrier frequencies for the sensor node and base-station. The sensor node transmits at 112MHz with a millimeter-scale antenna that results in a signal level well under the FCC limit at 3 meters due to cubic loss with distance in near-field. The base-station compensates the low sensor transmit power with a highly sensitive, low noise figure (~5dB) receiver. The base-station employs a transmitter with 30dBm output power at a less-optimal frequency of 49.86MHz to comply with U.S. FCC regulation.

The sensor transmitter operates at the battery voltage (4.1V) while the other blocks operate at 1.2V. The maximum current of the intended thin-film battery (~50μA) is insufficient to maximize the transmit efficiency. Thus we employ a 1.3nF on-chip decoupling capacitor (decap) as an energy-buffer which is continuously trickle-charged by the thin-film battery under protection of a current limiter. The decap allows high peak transmitter current, followed by idle time to recharge the decap. To exploit the resulting pulse sparsity, we propose a pulse-position modulation scheme (PPM) for the sensor node TX. The packet header from a sensor node consists of multiple pulses with a pseudo-random interval that is unique to that sensor node. The data message, on the other hand, is encoded in a binary PPM format. The base-station TX signal is modulated in continuous on-off keying. The sensor-node receiver consists of a 3-stage amplifier, envelope detector and clocked comparator. The comparator reference voltage is dynamically set by the baseband controller.

Figure 26.7.2 shows the sensor node wake-up timing diagram. The sleep power is 22nW and is dominated by the wake-up controller and the sleep timer (~10Hz). Periodically, or as instigated by the processor, the wake-up controller powers on the 200kHz baseband timer in two phases: First, the LDO inside the timer is stabilized for ~200ms while the VCO is clock-gated. Then, the VCO clock-gate is released and after ~1000 baseband cycles for frequency stabilization, the FastFSM wakes up the baseband controller. Interacting with the processor via MBUS [6], the baseband controller performs time-multiplexed modulation (TX) and demodulation (RX) with transceiver power-gating. Triggered by baseband controller signal 'BB_DONE', the system switches back to sleep mode where only the wake-up controller and sleep timer remain active. The 200kHz on-chip baseband timer employs a resistive frequency locking technique [7]. The baseband controller and timer consume 4.8μW active power in total.

The transmitter is based on a pulse-inject H-bridge LC-oscillator (Fig. 26.7.3), where the magnetic antenna and on-chip capacitors form a resonant tank. A conventional LC oscillator has low efficiency (~40% in simulation) due to constant tail current and power loss in the cross-coupled transistor pair. To increase efficiency, the proposed oscillator injects pulsed-current through an H-bridge only when oscillation is near peak. An inverter combined with a tunable pulse generator extracts and generates digital pulses from the oscillation signal. The inverter uses resistor bias at its gates to reduce short-circuit current. The proposed design utilizes two voltage domains (1.2V and 4.1V Vbat) to reduce overall power consumption. A switched-capacitor circuit is used for fast startup (Fig. 26.7.3, right). Two storage capacitors (charged to Vbat and ground separately) enable the tank (charged to Vbat/2) to oscillate during the first half cycle after which the oscillation is sustained by the pulse-inject loop. Simulated power efficiency of the proposed pulse-inject oscillator is 68%, which is 1.65x higher than the constant-bias oscillator. The startup time, a critical factor for an efficient pulsed-radio, is only 1 cycle.

We propose a new energy-efficient protocol where a sensor node initiates communication by transmitting a packet starting with multiple pulses with a predefined pseudo-random interval (i.e., header). Once the base-station detects a packet, it accurately estimates the baseband timing offset of the sensor node, adjusts its local timer frequency accordingly, and then sends a response packet after a precise, pre-defined guard time delay set by the sensor node timer. Since the packet (and data-symbol) arrival time is now synchronized to the sensor node baseband timer, the sensor node receiver no longer requires power-demanding timing offset estimation and symbol boundary synchronization. Note that in this scheme, it is the sensor node that periodically (using a wake-up timer) initiates communication with the base-station.

The full system is shown in Fig. 26.7.5. Our chip achieves longer link distance than other millimeter-scale near-field radios listed in Fig. 26.7.6. The transmitter consumes 43.5μw average power at 2kb/s. The received power at the 11x11cm^2 base-station antenna was -78dBm for a 50cm link including 3cm tissue. The sensor receiver achieved -54dBm sensitivity at 100kb/s with 36μW power and <3x10^{-3} target BER. This sensitivity was measured via a wired connection between an RF signal generator and the sensor receiver. The same BER was measured wirelessly with 20cm distance using a 1W base-station. Fig. 26.7.7 shows a die micrograph and summary of performance.

References:

[1] M. Mark et al., "A 1mm^3 2Mbps 330fJ/b Transponder for Implanted Neural Sensors," *IEEE Symp. VLSI Circuits,* pp. 168-169, June 2011.

[2] A. Yakovlev et al., "A 11μW Sub-pJ/bit Reconfigurable Transceiver for mm-Sized Wireless Implants," *IEEE Custom Integrated Circuits Conf.*, Sept. 2013.

[3] G. Chen et al., "A Cubic-Millimeter Energy-Autonomous Wireless Intraocular Pressure Monitor," *ISSCC Dig. Tech. Papers,* pp. 310-311, Feb. 2011.

[4] J. Bohorquez et al., "A 350 μW CMOS MSK Transmitter and 400 μW OOK Super-Regenerative Receiver for Medical Implant Communications," *IEEE J. Solid-State Circuits*, vol. 44, no. 4, pp. 1248-1259, Apr. 2009.

[5] A. Narayanan et al., "A Pulse-Driven LC-VCO with a Figure-of-Merit of -192dBc/Hz", *European Solid-State Circuits Conf.*, pp. 343-346, Sept. 2014.

[6] G. Kim et al., "A Millimeter-Scale Wireless Imaging System with Continuous Motion Detection and Energy Harvesting", *IEEE Symp. VLSI Circuits,* pp. 1-2, June 2014.

[7] M. Choi et al., "A 99nW 70.4kHz Resistive Frequency Locking On-Chip Oscillator with 27.4ppm/°C Temperature Stability", *IEEE Symp. VLSI Circuits.,* pp. C238-C239, June 2015.

 978-1-4673-9467-3/16/$31.00

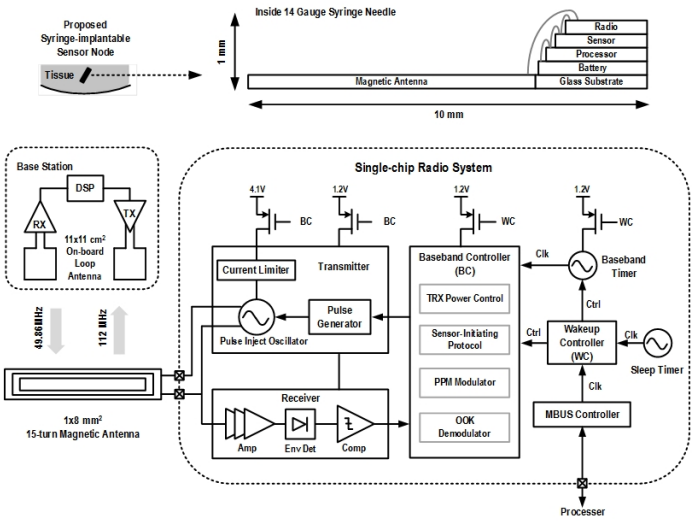

Figure 26.7.1: Syringe-implantable single-chip radio with 1x8mm² magnetic antenna on glass substrate.

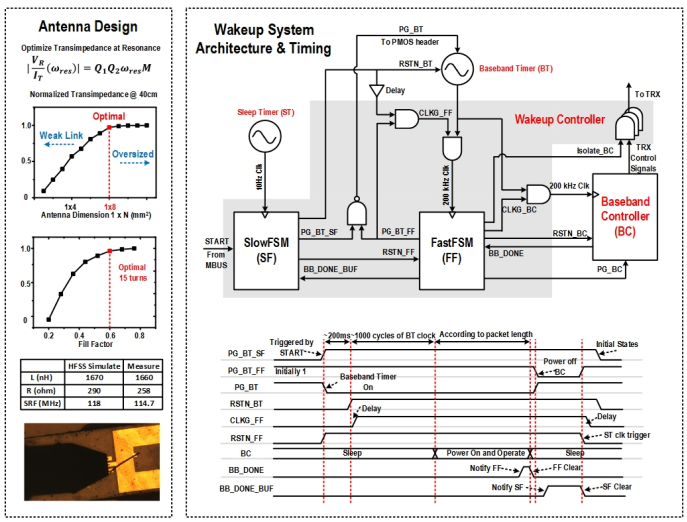

Figure 26.7.2: Design of asymmetric antennas. Architecture and timing diagram of wake-up system.

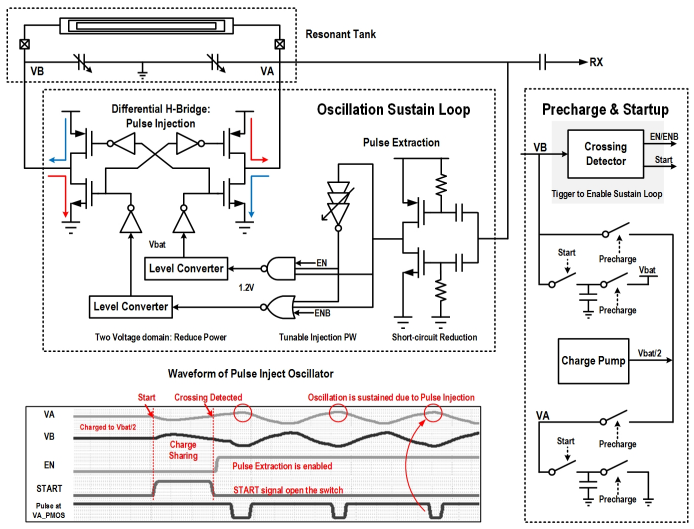

Figure 26.7.3: Architecture and waveform of pulse-inject H-bridge oscillator.

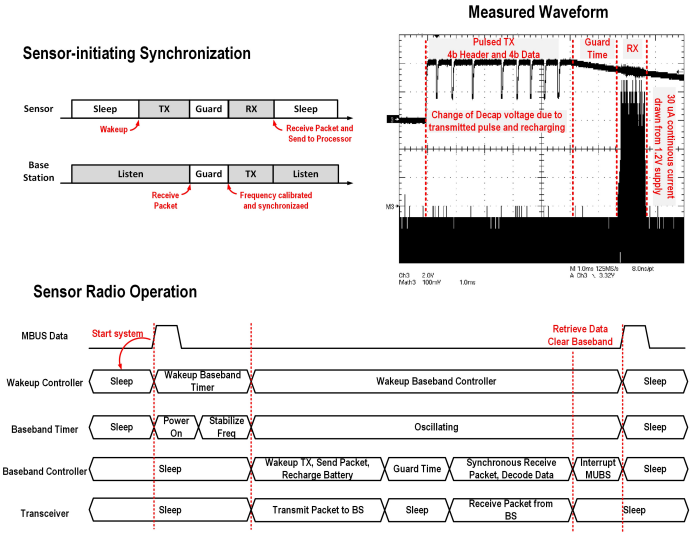

Figure 26.7.4: Sensor-initiating synchronization protocol.

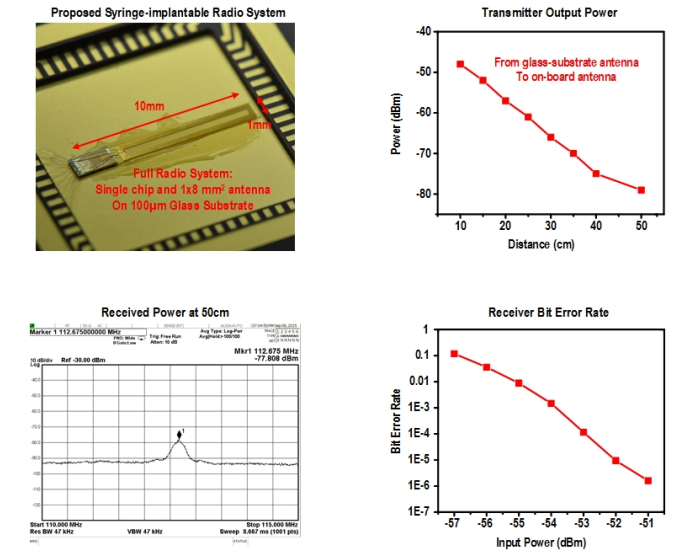

Figure 26.7.5: System photo and highlighted measurement results.

		This Work	CICC 2013 [2]	ISSCC 2011 [3]	VLSI 2011 [1]
Technology		180 nm	65 nm	180 nm	65 nm
Application		Syringe-implanted Sensors	Implanted Sensors	Intraocular Pressure Monitor	Implanted Neural Sensor
Antenna		1 x 8 mm² 15-turn	2 x 2 mm² 1-turn	0.4 x 0.4 mm² 6-turn	1.1 x 1.1 mm² 1-turn
Communicate Distance	Transmit	50 cm	3.5 cm	10 cm	1.3 cm
	Receive	20 cm	3.5 cm	N/A	N/A
Transmitter	Architecture	Pulse Injection LC Oscillator	Passive	Constant Bias LC Oscillator	Passive
	Center Frequency	112 MHz	1.32–2.14 GHz	570/690 MHz	535 MHz
	Modulation	PPM	LSK	FSK	LSK + PPM
	Peak Power	13.6 mW	1.4 µW	45.7 mW	660 nW
	Data Rate	2 kbps	2 Mbps	7.5 kbps	2 Mbps
Receiver	Sensitivity	-54 dBm @ 100kps	Unknown	N/A	N/A
	BER	1x10⁻³	Unknown		
	Center Frequency	49.86 MHz	1.32–2.14 GHz		
	Modulation	OOK	ASK		
	Power	36 µW	1.2 µW		
Baseband Controller and Clock		Integrated	N/A	N/A	N/A

Figure 26.7.6: Comparison with recent prior work.

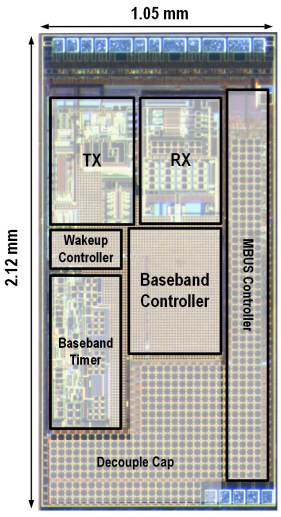

Technology		180nm CMOS
Die Area		2.12 x 1.05 mm^2
Transmitter	Average Power	43.5 µW @ 4.1V
	Peak Power	13.6 mW @ 4.1V
	Center Frequency	112 MHz
	Modulation	PPM
	Pulse Width	800 ns
	Data Rate	2 kbps
	Output Power	-78 dBm @ 50cm
Receiver	Active Power	36 µW @ 1.2V
	Center Frequency	49.86 MHz
	Modulation	OOK
	Data Rate	100 kbps
	Sensitivity	-54 dBm
	BER	10^{-3}
Baseband	Active Power	4.8 µW @ 1.2V
	Clock Frequency	200 kHz
System Sleep Power (Including Wake-up Controller)		22 nW

Figure 26.7.7: Die micrograph and summary of performance.

978-1-4673-9467-3/16/$31.00 ©2016 IEEE